16th World Conference on Earthquake, 16WCEE 2017
Santiago Chile, January 9th to 13th 2017
Paper N° 2811
Registration Code: S-N1464747123

Probabilistic Seismic Damage Analysis of Steel Self-Centering Concentrically Braced Frame Systems

E. Tahmasebi[(1)], R. Sause[(2)], J. M. Ricles[(3)]

[(1)] *Postdoctoral Research Associate, ATLSS Engineering Research Center, Lehigh University, U.S.A., tahmasebi@lehigh.edu*
[(2)] *Professor of Structural Engineering, ATLSS Engineering Research Center, Lehigh University, U.S.A., rs0c@lehigh.edu*
[(3)] *Professor of Structural Engineering, ATLSS Engineering Research Center, Lehigh University, U.S.A., jmr5@lehigh.edu*

Abstract

This paper develops damage scenario fragilities for buildings with either special concentrically braced frame (SCBF) system or a self-centering concentrically braced frame (SC-CBF) system as the seismic lateral force resisting system. A pre-event damage analysis is conducted using the damage scenario tree analysis (DSTA) technique and incremental dynamic analysis (IDA). The possibility of building demolition when collapse has not occurred is included in the DSTA. Three damage scenarios are considered: (i) building collapse; (ii) non-collapse with demolition; and (iii) non-collapse with non-demolition and component damage. Damage scenario fragilities for buildings with SCBF and SC-CBF systems are compared and discussed. The probabilities of damage to braces of the SCBF and SC-CBF at the maximum considered earthquake (MCE) hazard level are compared. Fragilities for the post tensioning bar damage scenarios for the buildings with the SC-CBF system are calculated and discussed.

.Keywords: self-centering; damage scenario tree; probabilistic damage analysis; braced frames; rocking frames

1 Introduction

Current building codes enables engineers to design for reduced earthquake forces by allowing nonlinear response (and consequently damage) under the design earthquake. This nonlinear response is usually in the form of yielding and buckling which lead to permanent deformations in structures. The innovative steel self-centering concentrically braced frame (SC-CBF) system is a new seismic lateral force resisting system that takes advantage of the efficiency of special concentrically braced frame (SCBF) system and also provides excellent ductility capacity without excessive permanent deformation due to the self-centering feature of the system.

The structural members of an SC-CBF system are similar to those of an SCBF system, namely columns, beams, and braces. In addition to these members, an SC-CBF has post tensioning (PT) bars running along the height of the structure which are anchored at the roof level and at the foundation. The main feature of an SC-CBF system is the ability to rock on its foundation after the column under tension from the overturning moment (i.e., the "tension" column) decompresses and uplifts from the foundation. The main restoring force, after the CBF rocks, is provided by pre-stressed PT bars. Decompression of the tension column and rocking of the SC-CBF lead to considerably softening of the lateral stiffness of the system. This softening of the SC-CBF lateral stiffness after column decompression reduces the earthquake forces. Unlike conventional seismic lateral force resisting systems, the original stiffness of an SC-CBF system is restored after the rocking motion is completed (e.g., at the end of earthquake shaking). Details of SC-CBF systems including possible configurations, design methods, and laboratory testing results can be found in [1-5].

Building collapse is often considered as the primary contributor to estimated earthquake-induced loss. In addition to collapse, structural and nonstructural damage during an earthquake which does not cause collapse of the building, but renders the building unoccupiable immediately after the earthquake, can also be a major contributor to the estimated loss [6]. A heavily damaged structure which has not collapsed during an earthquake may not be economical to repair and may need to be demolished [7, 8]. The consequences of heavy damage, in the form of residual deformation (e.g., residual story drift), is considered in previous research. For example Uma et al. [9] use the joint distribution of the maximum story drift ratio and residual story drift ratio to provide a three-dimensional performance matrix. Ramirez and Miranda [6] developed a loss estimation procedure that includes

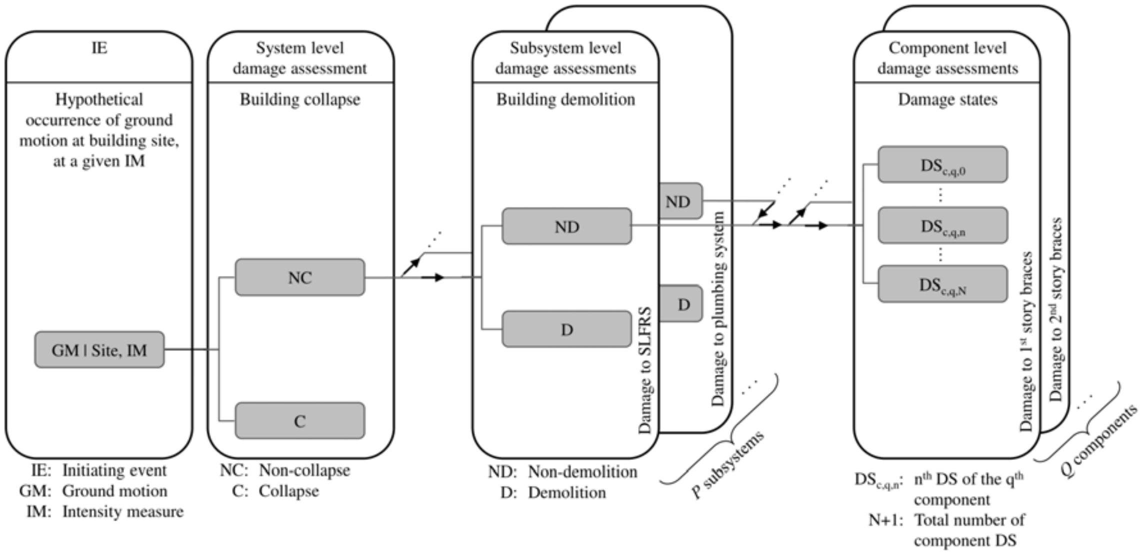

Fig. 1 Damage scenario tree diagram for probabilistic damage analysis of buildings

the residual story drift ratio and the resulting probability of demolition in the total estimated loss. Tahmasebi [10] organized damage assessment at the system level, subsystem level, and component level into a damage scenario tree diagram and developed fragilities for different damage scenarios.

This paper applies the damage scenario tree analysis (DSTA) developed by Tahmasebi [10], in the form of a pre-event damage analysis, to archetype buildings with SCBF and SC-CBF systems. Different damage scenarios of interest are presented and their fragilities are developed and compared. Demolition of the building when the building has not collapsed is considered. Damage assessment at the component level is performed for braces of SCBF and SC-CBF systems and the post tensioning bars of the SC-CBF system. Probabilities of damage scenarios including brace damage at maximum considered earthquake (MCE) hazard level are presented and discussed for both SCBF and SC-CBF systems.

2 Damage scenario tree analysis

A damage scenario tree analysis (DSTA) uses a hierarchy of levels for damage assessment [10]: (i) the entire system (i.e., the building); (ii) subsystems (e.g., the seismic lateral force resisting system of the building); and (iii) components (e.g., structural components such as columns, braces, and beams, or non-structural components such as cladding and partition walls). A damage scenario tree diagram is shown in Fig. 1. The initiating event (IE) in a DSTA could be a disruptive event such as an earthquake or a hurricane. In this paper the hypothetical occurrence of an earthquake ground motion at the building site, at a given hazard intensity level, is considered as the IE. The IE is followed by three assessment events (AE) at the system level, subsystem level, and component level of the building. Each AE is a probabilistic assessment of the damage state (DS) for the system, a subsystem, or a component.

Each AE has two or more resulting DS which form different branches of the damage scenario tree. The resulting DS for any given AE must be mutually exclusive and collectively exhaustive. A path from the IE to the end of a branch, including all the DS along the path, is called a *damage scenario*. Fig. 2 illustrates three damage scenarios from the damage scenario tree shown in Fig. 1. The probability of occurrence of a damage scenario (such as those shown in Fig. 2) is equal to the probability of the intersection of the DS at different levels, which form the damage scenario.

Seismic damage scenario fragilities are developed by quantifying the probability of each damage scenario at various seismic hazard intensity levels. Incremental dynamic analysis (IDA) [11] is used for predicting various engineering demand parameter (EDP) from structural response history analyses at increasing seismic hazard intensities. In this paper, the seismic hazard intensity measure (IM) is the 5% damped spectral acceleration at approximate fundamental period of the building, $S_a(T, 5\%)$. The far-field ground motion record set from FEMA P695 [12] is used for including the uncertainty due to record-to-record variability in structural response (denoted by RTR). Two DS of non-collapse (NC) and collapse (C) are considered at the system level damage assessment. At the subsystem level, two DS corresponding to non-demolition (ND) and demolition (D) of the building are considered. Two or more DS are considered for the component level damage assessment.

At the system level, the assessment of collapse DS is performed using an IM-based approach including the epistemic uncertainty in collapse criteria as described in [10]. At the subsystem level damage assessment, the seismic lateral force resisting system (SLFRS) of the building is considered as the only subsystem in the present study. The maximum (over all stories of the building) residual story drift ratio, θ_r, is used as the relevant EDP for quantifying the damage to the SLFRS of the building and the corresponding non-demolition or demolition repair actions.

At the component level, damage assessment is performed for the individual braces of the SLFRS (i.e., the SCBF or the SC-CBF). The probability of occurrence of each damage state is quantified using the residual out-of-plane displacement at the middle of the individual braces, Δ_{Or}, due to brace buckling, as the relevant EDP. Three brace DS are considered for individual braces: (i) no damage corresponding to no repair action (NR); (ii) slightly damaged corresponding to the brace straightening (BS) repair action; and (iii) heavily damaged corresponding to the brace replacement (BR) repair action. The probability of damage scenarios shown in Fig. 2 can be calculated as follows:

$$P(C|IM = im) = \sum_{all\ GM_l} F_{IM_{C,l}}(im) \cdot P(GM_l|IM = im) \tag{1}$$

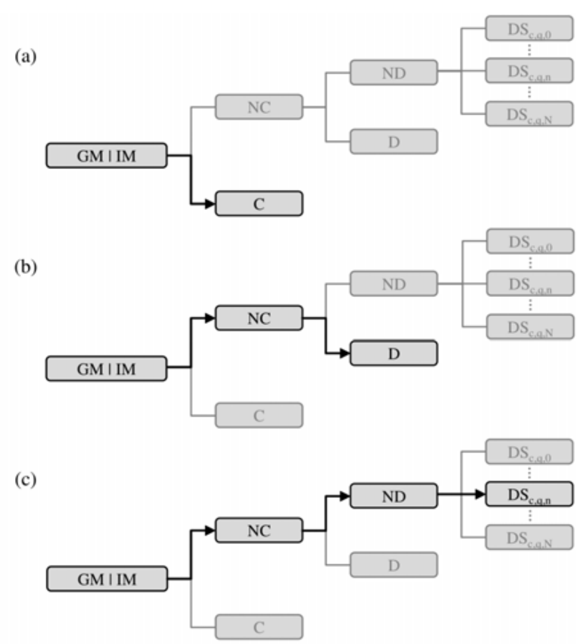

Fig. 2 Damage scenarios: (a) collapse ($C|IM$); (b) non-collapse with demolition ($NC \cap D|IM$); and (c) non-collapse, non-demolition with component damage ($NC \cap ND \cap DS_{c,q,n}|IM$)

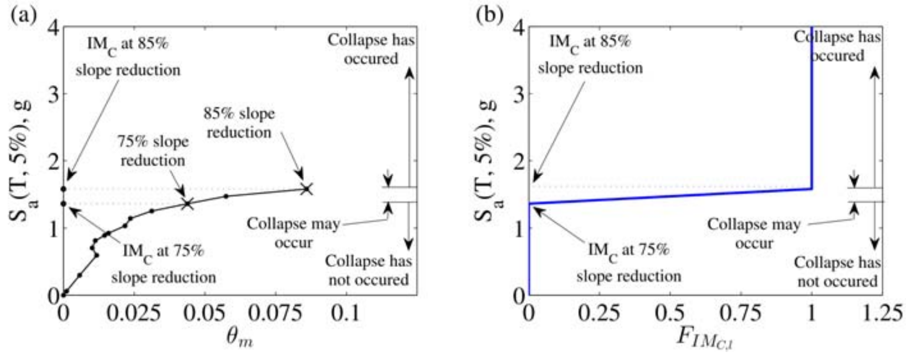

Fig. 3 IM-based method of quantifying collapse DS probability for a given GM_l with epistemic uncertainty in collapse DS slope reduction criterion: (a) IDA for GM_l; and (b) probability of collapse for GM_l (i.e.,$F_{IM_{C,l}}$)

$$P(NC \cap D|IM = im) = \sum_{all\ GM_l} \bar{F}_{IM_{C,l}}(im) \cdot F_{\theta_{r,D}}(\theta_{r,l}) \cdot P(GM_l|IM = im) \tag{2}$$

$$P(NC \cap ND \cap NR|IM = im) = \sum_{all\ GM_l} \bar{F}_{IM_{C,l}}(im) \cdot \bar{F}_{\theta_{r,D}}(\theta_{r,l}) \cdot (1 - F_{\Delta_{Or,DS,1}}(\Delta_{Or,l})) \cdot P(GM_l|IM = im) \tag{3}$$

$$P(NC \cap ND \cap BS|IM = im) = \sum_{all\ GM_l} \bar{F}_{IM_{C,l}}(im) \cdot \bar{F}_{\theta_{r,D}}(\theta_{r,l}) \cdot (F_{\Delta_{Or,DS,1}}(\Delta_{Or,l}) - F_{\Delta_{Or,DS,2}}(\Delta_{Or,l})) \cdot P(GM_l|IM = im) \tag{4}$$

$$P(NC \cap ND \cap BR|IM = im) = \sum_{all\ GM_l} \bar{F}_{IM_{C,l}}(im) \cdot \bar{F}_{\theta_{r,D}}(\theta_{r,l}) \cdot F_{\Delta_{Or,DS,2}}(\Delta_{Or,l}) \cdot P(GM_l|IM = im) \tag{5}$$

where $F_{IM_{C,l}}$ is the IM-based collapse fragility function for the l^{th} ground motion record from the ground motion record set, $F_{\theta_{r,D}}$ is the demolition fragility function, $F_{\Delta_{Or,DS,1}}$ is the brace straightening fragility function, $F_{\Delta_{Or,DS,1}}$ is the brace replacement fragility function, $\bar{F}$ are the complement of F (i.e., $\bar{F} = 1 - F$), and $P(GM_l|IM = im)$ is probability of occurrence of GM_l at a given im value. The detailed derivation of Eq. (1) through Eq. (5) can be found in [10].

3 Damage State Fragility Function

A key component in evaluation of Eq. (1) through Eq. (5) is the use of damage state (DS) fragility functions for calculating the probability of being in a DS and including the epistemic uncertainty corresponding to the DS. For the collapse DS, an IM-based fragility function is used for each individual ground motion record. The collapse of each archetype building subjected to a ground motion record is determined using the IDA results. The collapse point on the IDA point is established using two criteria: (i) reduction in the slope of the IDA curve (compared to the median initial slope of the IDA curves for the records in the record set); and (ii) maximum story drift ratio exceeding 10%. FEMA 355F [13] specifies 80% reduction in the IDA slope as the collapse point in an IDA. This slope reduction criterion for collapse is deterministic; namely, collapse certainly has not occurred for IM values at which 80% slope reduction has not occurred and collapse certainly has occurred for IM values at which the 80% slope reduction has occurred. Using this deterministic quantification of slope reduction criterion for collapse lead to establishment of a single collapse point on the IDA curve. The IM value corresponding to collapse point is the collapse capacity (denoted by IM_C) of the building under the ground motion record under consideration.

In this paper the epistemic uncertainty in slope reduction criterion is included by defining IM_C as a random variable over a range of IM values (rather than assigning a deterministic value) for any given ground motion. Three ranges of IM values are considered: (i) IM values at which the collapse certainly has not occurred; (ii) IM values at which the collapse may occur (i.e., the range for IM_C); and (iii) IM values at which the collapse certainly has occurred. The IM_C values inside the middle IM range are assumed to be uniformly distributed. Boundaries for the middle IM range (at which the collapse may occur) are established using two values of IDA slope reduction, 75% and 85%, as shown for one IDA curve in Fig. 3(a). A single IDA curve along with two marked points corresponding to 75% and 85% slope reduction are shown in Fig. 3(a). The three ranges of IM values are marked along the vertical axis. The IM-based collapse fragility function for the IDA of Fig. 3(a) is shown in Fig. 3(b). It can be seen that the value of $F_{IM_{C,l}}$ is zero for IM values less than IM_C at 75% slope reduction and is one for IM values greater than IM_C at 85% slope reduction. For IM values in between $F_{IM_{C,l}}$ varies linearly from zero to one. Subscript l in $F_{IM_{C,l}}$ shows that the collapse fragility function is defined for the l^{th} ground motion record and varies from record to record.

For the DS corresponding to demolition, an EDP-based fragility function is used to quantify the damage state probability. As stated previously, the maximum (over all stories) residual story drift ratio, θ_r, is used for quantifying the probability of demolition. The θ_r limit value that separate the two DS corresponding to non-demolition and demolition is denoted by $\theta_{r,D}$ and is defined as a random variable to include the DS epistemic uncertainty. A lognormal distribution is assumed for $\theta_{r,D}$ with a central value of 0.01 and a logarithmic standard deviation of 0.3. The demolition fragility function, denoted by $F_{\theta_{r,D}}$, is the cumulative distribution function (CDF) of such a distribution. The demolition fragility function is shown in Fig. 4(a). One $F_{\theta_{r,D}}$ is used for all ground motion records in Equations (2) through Eq. (5).

EDP-based fragility functions are also used to quantify the brace damage state probabilities. The residual displacement at the middle of the brace, Δ_{Or}, is used to quantify the probability of each brace damage state. Two Δ_{Or} limit values, denoted by $\Delta_{Or,DS,1}$ and $\Delta_{Or,DS,2}$, are defined as random variables and used for separating three brace DS. It is assumed that $\Delta_{Or,DS,1}$ and $\Delta_{Or,DS,2}$ follow a lognormal distribution with central values of 0.01 and 0.025 and logarithmic standard deviations of 0.25 and 0.3, respectively. The brace DS fragility functions separating the three brace DS are shown in Fig. 4(b).

4 Archetype Buildings

Four buildings with 4, 6, 9, and 12 stories are considered in this research. It is assumed that these buildings are office buildings, located in the Los Angeles area. The distribution of the seismic lateral resisting force system (SLFRS) in a typical floor plan of the buildings is shown in Fig. 5(a). The story height is 15 ft. for the first story and 13 ft. for stories other than the first story for all buildings.

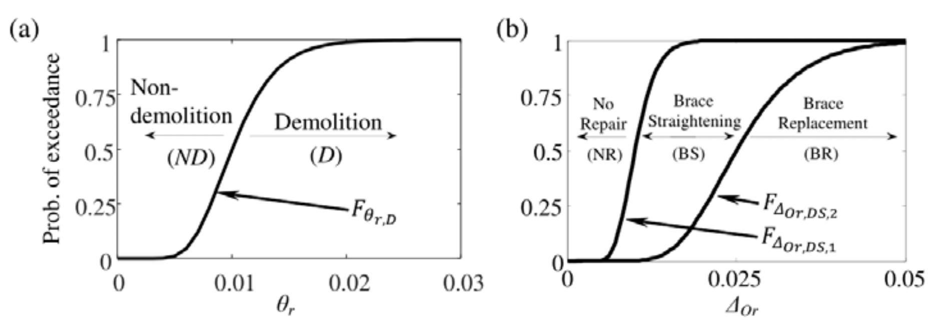

Fig. 4 Damage state fragility functions: (a) demolition fragility function $F_{\theta_{r,D}}$; and (b) brace damage state fragility functions $F_{\Delta_{Or,DS,1}}$ and $F_{\Delta_{Or,DS,2}}$

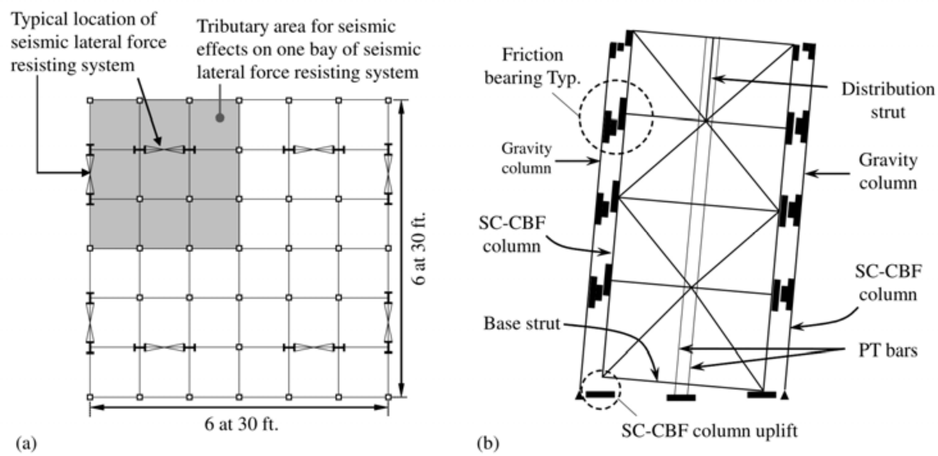

Fig. 5 Seismic lateral force resisting system in archetype buildings: (a) distribution in typical floor plan; and (b) schematic of different parts of a 4-story SC-CBF

Two types of SLFRS, a special concentrically braced frame (SCBF) and a self-centering concentrically braced frame (SC-CBF), are considered for each building. Considering the four buildings with different numbers of stories and the two types of SLFRS, a total of eight different *archetype buildings* with different numbers of stories and SLFRS are studied. To distinguish between different archetype buildings, unique names are assigned to them using the number of stories and the type of SLFRS. The names of the SCBF archetype buildings are 4SCBF, 6SCBF, 9SCBF, and 12SCBF. Similarly, the names of the SC-CBF archetype buildings are 4SC-CBF, 6SC-CBF, 9SC-CBF, and 12SC-CBF. For each archetype building, a one-bay SLFRS and the seismic mass and seismic weight tributary to the one-bay SLFRS (as shown in Fig. 5(a) for a typical floor plan) are modeled numerically, based on the symmetry of the building.

The SCBF system studied in this research is the special steel concentrically braced frame SLFRS, as listed and defined in ASCE 7-10 [14]. It consists of beams, columns, and braces in a conventional (2-story X bracing) configuration. The members of the SCBF system are designed to satisfy the ASCE 7-10 [14] seismic design criteria and also the AISC seismic provisions for structural steel buildings [15].

The SC-CBF system is an innovative SLFRS [3] consisting of beams, columns, and braces in a conventional arrangement similar to an SCBF system. In contrast with the SCBF system, the column base detail of the SC-CBF system permits the column to uplift at the foundation and rock [16]. A schematic configuration of SC-CBF system is shown in Fig. 5(b). Post-tensioning (PT) bars are anchored to the SC-CBF beam at the roof level and at the foundation. The SC-CBF system can have one or more distribution strut(s) to distribute the force from the PT bars (anchored at the roof level) to the braces over several stories, as shown in Fig. 5(b). Also, a base strut is included at the base of the SC-CBF system to transfer the base shear to the SC-CBF column base which is in contact with the foundation.

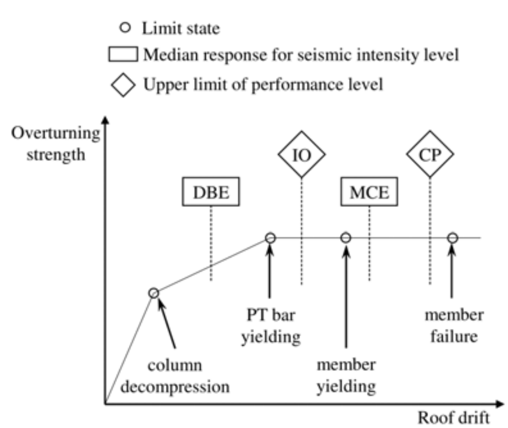

Fig. 6 Schematic representation of SC-CBF limit states and performance objectives, from [3]

The SC-CBF deforms elastically similar to a conventional SCBF under low levels of lateral force. Under high levels of lateral force, the overturning moment at the base of the frame becomes large enough for the "tension" column to decompress, and uplift of the column occurs, as shown schematically in Fig. 5(b). To enable the column uplift and rocking of the SC-CBF, the beams of SC-CBF are not connected to the floor diaphragm at each floor level and can freely move in the vertical direction as the SC-CBF rocks. Therefore, the gravity loads on floor levels adjacent to the SC-CBF are not transferred to the SC-CBF beams, rather, they are carried by the so-called gravity columns adjacent to the SC-CBF. The only vertical load applied to the SC-CBF is the self-weight of the SC-CBF structural members (i.e., beams, columns, braces, etc.) [16].

The SCBF systems are designed using the equivalent lateral force (ELF) method of ASCE 7-10 [14], and the AISC seismic design provisions for structural steel buildings [15]. The SC-CBF systems are designed using a modal response spectrum analysis (RSA) method with modifications proposed by Roke et al. [17] and improvements proposed by Chancellor [18]. The RSA requires the mode shapes and periods of vibration for the structural system, which are determined from an eigenvalue analysis. This eigenvalue analysis was performed on a linear elastic model of the SC-CBF with the tributary seismic mass and gravity load system (represented as a lean-on-column). The SC-CBF columns are fixed at the base in this linear model. The modal lateral forces are determined for a sufficient number of modes, with at least 90% of the total seismic mass included in the modal mass for these modes. The modal responses are combined using a modal combination method [18]. Members of the SCBF and SC-CBF are designed using wide flange sections for all archetype buildings.

The main design objective for the SC-CBF system is to be damage free under the design basis earthquake (DBE) and an SC-CBF building is intended to remain functional so that it can be immediately occupied after the earthquake. This performance objective is different from the standard seismic design performance objective of life-safety under the DBE. The SC-CBF design procedure targets a performance objective of immediate occupancy (IO) under the DBE and a performance objective of collapse prevention (CP) under the maximum considered earthquake (MCE). Schematic relationships between SC-CBF limit states and SC-CBF design performance objectives are shown in Fig. 6. Four limit states of column decompression (followed by rocking), PT bar yielding, member yielding, and member failure are shown in Fig. 6. Member yielding should not occur before PT bar yielding.

The PT bar yielding limit state can have different consequences depending on the amount of yielding that occurs. Yielding of the PT bars causes loss of the initial post-tensioning force in the PT bars. With limited PT bar yielding, the SC-CBF still self-centers without significant damage and the IO performance objective is still achievable. Therefore, the SC-CBF system is designed so the median DBE response occurs without PT bar yielding. For response under the DBE greater than the median response, limited PT bar yielding is expected.

5 Numerical Models for Structural Analyses

Numerical modeling and nonlinear response analyses are carried out using the OpenSees computational framework [19]. A two dimensional finite element model of the one-bay SLRFS (i.e., SCBF or SC-CBF) is developed for each archetype SLFRS in OpenSees. The seismic mass and gravity load, tributary to the one-bay SLFRS are included in the finite element model. The second order effect of the gravity load, the so-called P-Δ effect, is simulated using a lean-on-column. Gravity loads are applied to the lean-on-column at each floor level to include the P-Δ effect during the static pushover analyses and the dynamic response history analyses. The lean-on-column gravity loads are determined from the combination of dead load (DL) and live load (LL) as 1.05 DL + 0.25 LL [12]. The seismic mass is determined from the dead load and the partition load.

Material and geometric nonlinearity are considered in the finite element models. The Menegotto-Pinto hysteresis model is used for the structural steel material. Strength and stiffness deterioration due to buckling is used in the modeling of the braces. The braces are modeled with 16 beam column elements per member and an initial lateral imperfection of 1/1000 of the brace length at the middle of the braces to initiate brace buckling, using the approach of Uriz et al. [20]. Fracture of the brace members due to low-cycle fatigue, induced by local buckling, is simulated using a rainflow cycle counting method as described by Uriz [21]. Such local buckling is not directly modeled. The "corotational" geometric transformation in OpenSees is used for the brace elements to enable simulation of large deformation and buckling of the brace members. While the columns are modeled without initial imperfection, column buckling is allowed by using 4 elements per column and the corotational transformation for the column elements. Deformation of a column member (i.e., a deviation from the initially perfectly straight transverse position of the column) during a static pushover analysis or a dynamic response history analysis is similar to the initial imperfection in a brace member. Therefore, when the combination of column transverse deformation, axial force, and bending moment reaches a critical limit (of instability), buckling occurs in a column member. Buckling is prevented for the beam members of the SCBF archetype SLFRS by using a "linear" geometric transformation for the beam elements, as the beams are laterally supported by the floor diaphragm for the SCBF archetype buildings. Buckling is allowed for the beam members of the SC-CBF archetype SLFRS by using 4 elements per beam and a corotational geometric transformation for the beam elements, similar to the column members.

6 Damage Scenario Fragilities

Damage scenario fragilities are plots of the probability of occurrence of a damage scenario versus various IM values. In this section the fragilities for damage scenarios shown in Fig. 2 are presented and discussed. At the component level, the damage scenarios including the damage to the braces of the SCBF and SC-CBF are discussed and compared. Also the damage scenario fragilities including PT bars damage for the SC-CBF archetype buildings are discussed and presented.

6.1 Collapse (C) damage scenario

The fragilities for the collapse (C) damage scenario for all archetype buildings are shown in Fig. 7. These fragilities are developed by evaluating Eq. (1) at various $S_a(T, 5\%)$ values. It can be seen from Fig. 7 that the probability of collapse for the SC-CBF archetype buildings is less than the probability of collapse for the SCBF archetype buildings at all $S_a(T, 5\%)$ values. It can also be seen that the probability of collapse at the MCE hazard intensity is negligible.

6.2 Non-collapse with demolition ($NC \cap D$) damage scenario

The fragilities for the non-collapse with demolition ($NC \cap D$) damage scenario are shown in Fig. 8. These fragilities are developed by evaluating Eq. (2) at various $S_a(T, 5\%)$ values. It can be seen from Fig. 8 that $P(NC \cap D)$ is close to zero at small the $S_a(T, 5\%)$ values, increases as the $S_a(T, 5\%)$ values increase, reaches a peak value, and finally decreases to zero as $S_a(T, 5\%)$ values decrease. Such a trend of increase and then decrease in $P(NC \cap D)$ is different from the monotonically increasing trend of $P(C)$. This trend of $P(NC \cap D)$ becomes clear by looking at components of Eq. (2). At small $S_a(T, 5\%)$ values the probability of demolition, quantified by $F_{\theta_{r,D}}$, is close to zero because the residual story drift ratio (θ_r) values are negligible as seen from Fig. 4(a) (i.e., $F_{\theta_{r,D}}\ (\theta_r) \approx 0$). As a result $P(NC \cap D)$ is negligible at small $S_a(T, 5\%)$ values. The probability of non-collapse, quantified by $\bar{F}_{IM_{C,l}}$, is close to zero at large $S_a(T, 5\%)$ values for all ground motion records (GM_l). As a result, $P(NC \cap D)$ becomes negligible at large $S_a(T, 5\%)$ values. Therefore, the increasing and then decreasing trend of $P(NC \cap D)$ with increasing $S_a(T, 5\%)$ is due to the multiplication of two components; one that increases and another that decreases with increasing $S_a(T, 5\%)$.

At $S_a(T, 5\%)$ values where probability of non-collapse and probability of demolition are not negligible, $P(NC \cap D)$ has non-zero values. At these $S_a(T, 5\%)$ values the increasing part of the $NC \cap D$ fragility is more affected by $F_{\theta_{r,D}}$ as $\bar{F}_{IM_{C,l}}$ is close to 1; and the decreasing part of the $NC \cap D$ fragility is more affected by $\bar{F}_{IM_{C,l}}$ as $\bar{F}_{IM_{C,l}}$ is close to 1.

It can be seen from Fig. 8 that the $NC \cap D$ damage scenario fragilities for the SC-CBF archetype buildings are to the right side of the fragilities for the SCBF archetype buildings. This shift to the right shows that the non-negligible probabilities of the $NC \cap D$ damage scenario are shifted to greater hazard level for the SC-CBF archetype buildings. For all archetype buildings the value of $P(NC \cap D)$ at the MCE hazard intensity for the SCBF

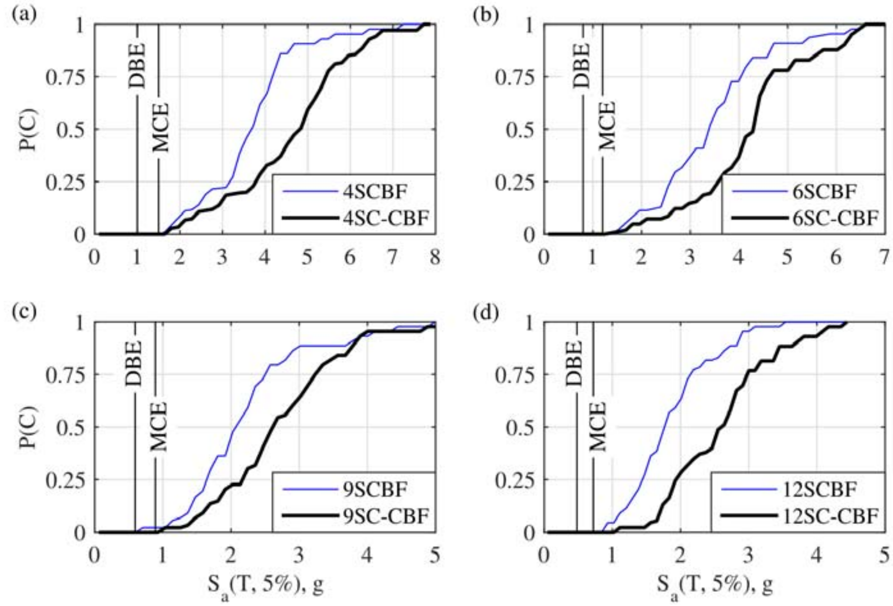

Fig. 7 Fragility for collapse (C) damage scenario for: (a) 4-story archetype buildings; (b) 6-story archetype buildings; (c) 9-story archetype buildings; and (d) 12-story archetype buildings

system is greater than that of the SC-CBF system. The value of $P(NC \cap D)$ at the DBE hazard intensity is negligible for all archetype buildings.

At larger $S_a(T, 5\%)$ values, i.e., $S_a(T, 5\%) \geq$ 3.5g, 3g, 2g, and 2g in Fig. 8(a), (b), (c), and (d), respectively, $P(NC \cap D)$ for the SC-CBF system becomes greater than $P(NC \cap D)$ for the SCBF system. The smaller $P(NC \cap D)$ values for the SCBF system is caused by considerably greater $P(C)$ values at larger $S_a(T, 5\%)$ values for the SCBF system compared to the SC-CBF systems. Looking at the fragilities for C damage scenario in Fig. 7, it can be seen that at the aforementioned $S_a(T, 5\%)$ values, $P(C)$ for the SCBF system is considerably greater than $P(C)$ for the SC-CBF system.

6.3 Brace damage scenarios

When the building is not collapsed and the induced damage does not require the demolition of the building, structural and non-structural component damage scenarios become relevant. In this paper damage to bracing members of the SCBF and SC-CBF systems are considered. Fragilities for the damage scenarios shown in Fig. 9(c) can be developed for each bracing member and all brace DS considered. As stated previously, three brace DS corresponding to no repair action (NR), brace straightening (BS), and brace replacement (BR) are considered for a bracing member.

Fig. 9 shows the fragilities for the first story brace damage scenarios of the 9SCBF and 9SC-CBF archetype buildings. The fragility for the $NC \cap ND \cap NR$ damage scenario is shown in Fig. 9(a), (b). These fragilities are obtained by evaluating Eq. (3) at various $S_a(T, 5\%)$ values. It can be seen that $P(NC \cap ND \cap NR)$ decreases as $S_a(T, 5\%)$ increases. Such a decrease is expected as $\bar{F}_{IM_{C,l}}$, $\bar{F}_{\theta_{r,D}}$, and $(1 - F_{\Delta_{Or,DS,1}})$, three components of Eq. (3) that are a function of $S_a(T, 5\%)$, generally decrease with increase of $S_a(T, 5\%)$. It is clear from Fig. 9(a), (b) that the first story braces of the 9SCBF archetype building have a high probability of damage compared to the first story braces of the 9SC-CBF archetype building. Similar differences between $P(NC \cap ND \cap NR)$ values for other braces and other archetype buildings (with the same number of stories) are observed. The $NC \cap ND \cap NR$ damage scenario fragilities for other stories and other archetype buildings are not presented in this paper for brevity.

The fragilities for the $NC \cap ND \cap BS$ damage scenario are shown in Fig. 9(c) and (d). These fragilities are obtained by evaluating Eq. (4) at various $S_a(T, 5\%)$ values. The variation of the $NC \cap ND \cap BS$ fragility with $S_a(T, 5\%)$ is similar to the $NC \cap D$ fragility. Namely, $P(NC \cap ND \cap NR)$ increases from zero at small $S_a(T, 5\%)$ values, stays non-negligible for a certain range of $S_a(T, 5\%)$ values, and decreases to zero as $S_a(T, 5\%)$ increases.

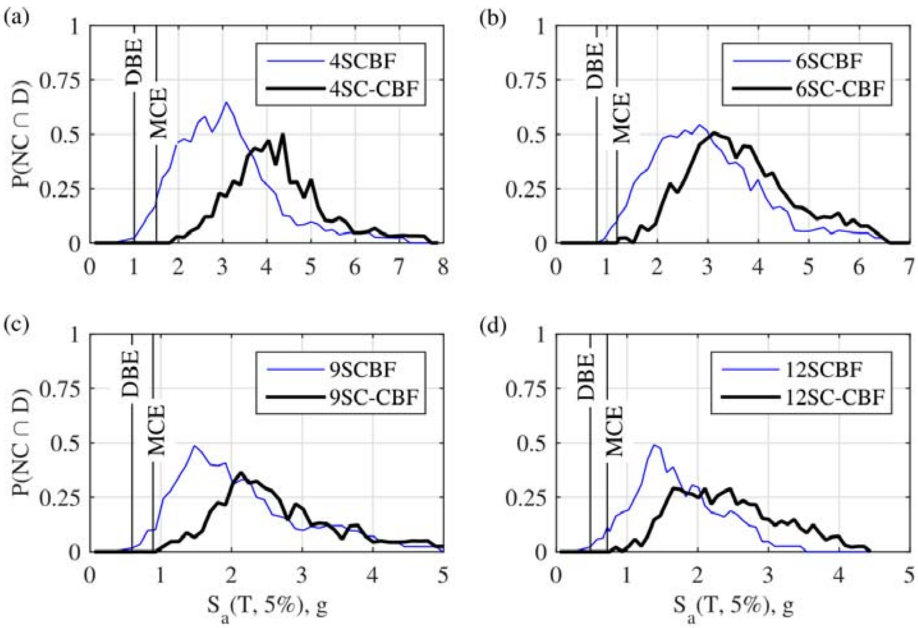

Fig. 8 Fragility for non-collapse with demolition ($NC \cap D$) damage scenario for: (a) 4-story archetype buildings; (b) 6-story archetype buildings; (c) 9-story archetype buildings; and (d) 12-story archetype buildings

This trend is caused by the $F_{\Delta_{Or,DS,1}}(\Delta_{Or,l}) - F_{\Delta_{Or,DS,2}}(\Delta_{Or,l})$ component of Eq. (4). Looking at Fig. 4(b), it can be seen that the difference of the two brace DS fragility functions is close zero at small Δ_{Or} values, non-zero at intermediate Δ_{Or} values, and is again close zero at large Δ_{Or} values. Note that the Δ_{Or} value generally increases as $S_a(T, 5\%)$ increases in an IDA, which explains the trend of the $NC \cap ND \cap BS$ damage scenario fragility as $S_a(T, 5\%)$ increases. The $\bar{F}_{IM_{C,l}}$ and $\bar{F}_{\theta_{r,D}}$ components of Eq. (4) decrease when $S_a(T, 5\%)$ increases.

Looking at Fig. 9(c) and (d) at the MCE hazard level, it can be seen that the $P(NC \cap ND \cap BS \mid IM = S_{MT})$ value for the first story braces are negligible for the 9SC-CBF archetype building but are not negligible for the 9SCBF archetype building. The $NC \cap ND \cap BS$ fragilities for other braces are not shown in this paper for brevity. However the values of $P(NC \cap ND \cap BS)$ at the MCE hazard level are negligible for most of the braces of the SC-CBF archetype buildings but are not negligible for the braces of the SCBF archetype buildings.,

The fragilities for the $NC \cap ND \cap BR$ damage scenario are shown in Fig. 9(e) and (f). These fragilities are obtained by evaluating Eq. (5) at various $S_a(T, 5\%)$ values. Similar to the $NC \cap ND \cap BS$ and $NC \cap D$ fragilities, the fragility for $NC \cap ND \cap BR$ increases from zero at small $S_a(T, 5\%)$ values, and stays non-negligible over a range of $S_a(T, 5\%)$ values and then decreases to zero as $S_a(T, 5\%)$ increases. Similar to $NC \cap D$ damage scenario fragility, this trend is caused by multiplying a decreasing component by an increasing component. The $\bar{F}_{IM_{C,l}} \cdot \bar{F}_{\theta_{r,D}}$ component decreases and the $F_{\Delta_{Or,DS,2}}$ component increases with increase of $S_a(T, 5\%)$. It can be seen from Fig. 9(e) and (f) that the $P(NC \cap ND \cap BS)$ values for the first story braces are negligible for the 9SC-CBF archetype building but are not negligible for the 9SCBF archetype building. Similar differences are observed between the braces of the SC-CBF and SCBF archetype buildings with different numbers of stories.

7 Conclusions

A pre-event damage analysis is conducted using the damage scenario tree analysis (DSTA) technique for archetype buildings with special concentrically braced frame (SCBF) and self-centering concentrically braced frame (SC-CBF) systems in this paper. Damage scenarios of collapse, non-collapse with demolition, and non-collapse with non-demolition and component damage are studied. Damage to the braces of the SCBF and SC-CBF systems are considered at the component level. Also, damage to the post tensioning (PT) bars of the SC-CBF system are considered at the component level.

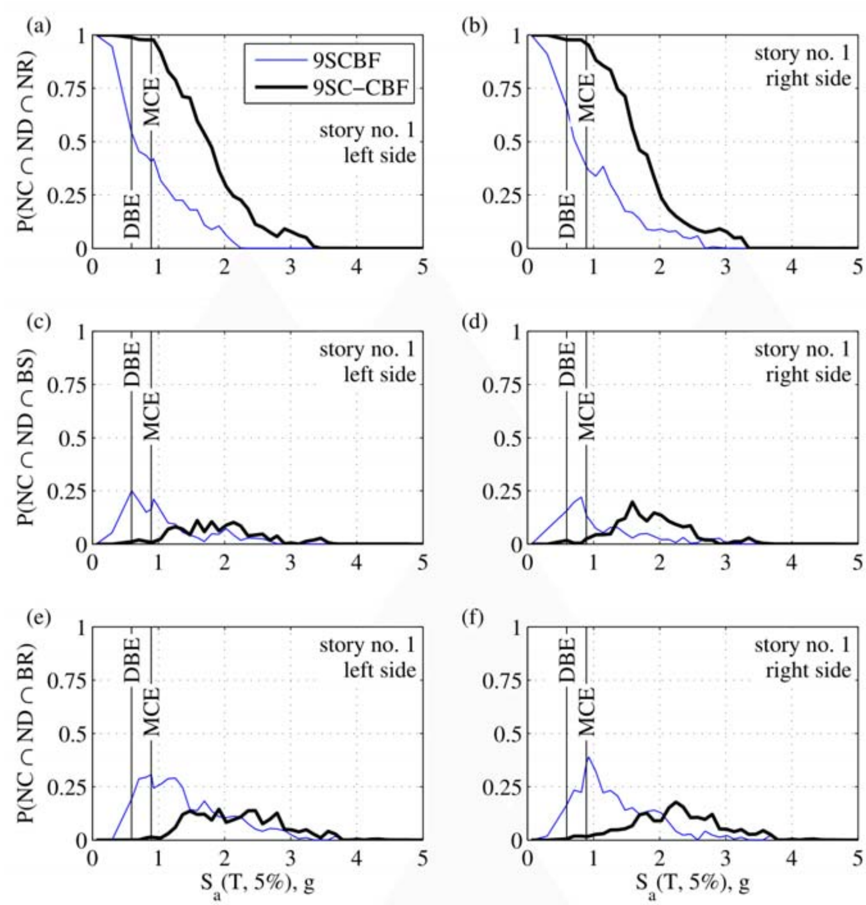

Fig. 9 Comparison of brace damage scenario fragilities for 1st story of 9-story archetype buildings: (a) $NC \cap ND \cap NR$ for left side brace; (b) $NC \cap ND \cap NR$ for right side brace; (c) $NC \cap ND \cap BS$ for left side brace; (d) $NC \cap ND \cap BS$ for right side brace; (e) $NC \cap ND \cap BR$ for left side brace; and (f) $NC \cap ND \cap BR$ for right side brace

It is observed that the probability of collapse for the SC-CBF archetype buildings is smaller than the probability of collapse for the SCBF archetype buildings, with a similar number of stories, at all $S_a(T, 5\%)$ values. The probability of collapse is observed to be negligible at the DBE and MCE hazard level for the SCBF and the SC-CBF archetype buildings. It is also observed that fragilities for the non-collapse with demolition damage scenario for the SC-CBF archetype buildings are shifted towards the larger $S_a(T, 5\%)$ values compared to the SCBF archetype buildings. This shift shows that a larger $S_a(T, 5\%)$ value, corresponding to more intense GM or greater seismic hazard, is needed to produce the same damage scenario (non-collapse with demolition) probability for the SC-CBF archetype buildings compared to the SCBF archetype buildings. The probability of non-collapse with demolition is observed to be negligible at the DBE hazard level for the SCBF and the SC-CBF archetype buildings. At the MCE hazard level, the probability of non-collapse with demolition is observed to be negligible for the SC-CBF archetype buildings but non-negligible for the SCBF archetype buildings.

The probabilities for the damage scenarios including brace damage are observed to be considerably smaller for the SC-CBF archetype buildings in comparison with the SCBF archetype buildings. The number of stories with negligible probability of brace damage at the MCE hazard level was considerably larger for the SC-CBF archetype buildings than for the SCBF archetype buildings.

8 References

[1] D. Roke, R. Sause, J. M. Ricles, C.-Y. Seo and K.-S. Lee, "Self-Centering Seismic-Resistant Steel Concentrically-Braced Frames," in *Proceedings of 8th US National Conference on Earthquake Engineering*, San Francisco, California, 2006.

[2] N. Gonner, N. B. Chancellor, R. Sause, J. M. Ricles, D. Roke and J. Miranda, "Design, Experimental Setup, and Testing of Self-Centering Steel Concentrically-Braced Frame Test Structure," ATLSS Report 10-06, Lehigh University, Bethlehem, Pennsylvania, 2010.

[3] D. A. Roke, "Damage-free seismic-resistant self-centering concentrically-braced frames," PhD Dissertation, Department of Civil and Environmental Engineering, Lehigh University, Bethlehem, PA, 2010.

[4] M. Eatherton, J. Hajjar, X. Ma, H. Krawinkler and G. Deierlein, "Seismic Design and Behavior of Steel Frames with Controlled Rocking – Part I: Concepts and Quasi-Static Subassembly Testing," in *Structures Congress*, Orlando, FL, 2010a.

[5] X. Ma, M. Eatherton, J. Hajjar, H. Krawinkler and G. Deierlein, "Seismic Design and Behavior of Steel Frames with Controlled Rocking–Part II: Large Scale Shake Table Testing and System Collapse Analysis," in *Structures Congress*, Orlando, FL, 2010.

[6] C. M. Ramirez and E. Miranda, "Significance of residual drifts in building earthquake loss estimation," *Earthquake Engineering & Structural Dynamics,* vol. 41, no. 11, pp. 1477-1493, 2012.

[7] E. Rosenblueth and R. Meli, "The 1985 earthquake: causes and effects in Mexico City," *Concrete International,* vol. 8, no. 5, pp. 23-34, 1986.

[8] K. Kawashima, "Seismic design and retrofit of bridges," in *Proceedings of the Twelfth World Conference on Earthquake Engineering*, Auckland, 2000.

[9] S. R. Uma, S. Pampanin and C. Christopoulos, "Development of probabilistic framework for performance-based seismic assessment of structures considering residual deformations," *Journal of Earthquake Engineering,* vol. 14, no. 7, pp. 1092-1111, 2010.

[10] E. Tahmasebi, "Damage Assessment of Steel Concentrically Braced Frame Systems under Seismic Conditions," PhD Dissertation, Department of Civil and Environmental Engineering, Lehigh University, Bethlehem, PA, 2016.

[11] D. Vamvatsikos and C. A. Cornell, "Incremental Dynamic Analysis," *Earthquake Engineering & Structural Dynamics,* vol. 31, no. 3, pp. 491-514, 2002.

[12] FEMA, "Quantification of Building Sismic Performance Factors," Federal Emergency Management Agency, FEMA P695, Washington, DC, 2009.

[13] FEMA, "State of art report on performance prediction and evaluation of steel moment-frame buildings," Federal Emergency Management Agency, Report No. FEMA-355F, Washington, DC, 2000.

[14] ASCE, "Minimum Design Loads for Buildings and Other Structures," ASCE/SEI 7-10, Reston, Virginia, 2010.

[15] AISC, "Seismic Provisions for Structural Steel Buildings," ANSI/AISC 341-10, Chicago, Illinois, 2010.

[16] R. Sause, J. M. Ricles, D. Roke, C.-Y. Seo and K.-S. Lee, "Design of self-centering steel concentrically-braced frames," in *Proc. Of Sessions of the 4th International Conference on Earthquake Engineering*, Taipei Taiwan, 2006.

[17] D. Roke, R. Sause, J. M. Ricles and N. Gonner, "Design concepts for damage-free seismicresistant self-centering steel concentrically-braced frames," in *Proceedings of the 14th World Conference on Earthquake Engineering*, Beijing, China, 2008.

[18] N. B. Chancellor, "Seismic Design and Performance of Self-Centering Concentrically-Braced Frames," PhD Dissertation, Department of Civil and Environmental Engineering, Lehigh University, Bethlehem, PA, 2014.

[19] F. McKenna, "Object-oriented finite element programming: frameworks for analysis, algorithms and parallel computing," PhD dissertation, University of California at Berekeley, Berekeley, California, 1997.

[20] P. Uriz, F. C. Filippou and S. A. Mahin, "Model for Cyclic Inelastic Buckling of Steel Braces," *Journal of Structural Engineering,* vol. 134, no. 4, pp. 619-628, 2008.

[21] P. Uriz, "Toward Earthquake-Resistant Design of Concentrically Braced Steel-Frame Structures," PhD Diss., University of California at Berkeley, Berkeley, California, 2005.

[22] F. J. Perez, S. Pessiki and R. Sause, "Experimental and analytical lateral load response of unbonded post-tensioned precast concrete walls," ATLSS Report No. 04-11, ATLSS Engineering Research Center, Lehigh University, Bethlehem, PA, 2004.